Research on Chemical Intermediates (2022) 48:2973–2986
https://doi.org/10.1007/s11164-022-04741-6

Fabrication of 5-aryl-1*H*-tetrazoles derivatives by solid-state synthesized $MgFe_2O_4$ and $MgFe_2Zn_xO_{4+\delta}$ heterogeneous nanocatalysts

Leila Kafi-Ahmadi[1] · Shahin Khademinia[2] · Ahmad Poursattar Marjani[3] · Peyman Gozali Balkanloo[3]

Received: 2 March 2022 / Accepted: 11 May 2022 / Published online: 10 June 2022

Abstract

$MgFe_2O_4$ and $MgFe_2Zn_xO_{4+\delta}$ composite samples were fabricated using $MgCl_2.6H_2O$ and $FeCl_3.6H_2O$ (and $Zn(NO_3)_2.6H_2O$ for the doped sample) in one-step, solid-state reactions at 800 °C for 12 h. The obtained materials were characterized by the powder X-ray diffraction technique. Rietveld analysis data showed that the obtained $MgFe_2O_4$ was crystallized in the cubic crystal system with the space group Fd-3m. The morphology of the synthesized materials was studied by a field emission scanning electron microscope. The aim of the present work was the preparation of 5-aryl-1*H*-tetrazoles from benzonitrile raw material derivatives and sodium azide in the presence of $MgFe_2O_4$ and $MgFe_2Zn_xO_{4+\delta}$ heterogeneous and recyclable catalysts under conventional heating conditions. The main superiorities of the method were high output and simplicity. Time, temperature, solvent type, and quantity of the catalyst were considered crucial factors for optimization of the reaction conditions. According to the results, the best conditions for the catalytic reaction were 3 h, 80 °C, 5 mol% catalyst, and dimethyl sulfoxide solvent. At the optimum conditions, a high catalytic yield (97%) was obtained.

✉ Leila Kafi-Ahmadi
l.kafiahmadi@urmia.ac.ir

[1] Department of Inorganic Chemistry, Faculty of Chemistry, Urmia University, Urmia, Iran

[2] Department of Inorganic Chemistry, Faculty of Chemistry, Semnan University, Semnan, Iran

[3] Department of Organic Chemistry, Faculty of Chemistry, Urmia University, Urmia, Iran

Graphical abstract

Keywords Heterogeneous catalyst · Nanoparticles · Zn-doped $MgFe_2O_4$ · 5-Aryl-1*H*-tetrazoles

Introduction

Heterogeneous catalysts with a nano-scale structure exhibit high efficiency and selectivity in organic transformations [1]. They can be isolated and separated readily from the desired organic compounds. Besides, they are recyclable and reusable while maintaining their catalytic properties [2, 3]. Recently, magnetic nanomaterials have attracted plenty of interest due to their extensive potential applications like catalytic reactions, magnetic resonance imaging, biomedicine, data storage, and batteries [4]. Recently, Fe-based oxides such as MFe_2O_4 (M = Co, Ni, and Mn) have drawn more attention due to their green chemistry, optical properties, photocatalytic features, and wide ranges of chemical composition [5, 6]. They are magnetically soft and possess *n*-type semiconductor features. Their properties are favorable to use in heterogeneous catalysts, sensors, and other high-tech magnetic applications [7]. Magnesium ferrite ($MgFe_2O_4$) has been used as a catalyst for various applications such as carbon production, water purification, alkylation, dehydrogenation, dechlorination, oxidation [8–10]. The physical properties are affected by different factors such as structure, stoichiometry, particle porosity, grain size, and ion distribution in the system [11]. In the last years, the metallic ions such as Al, Cd, Cr, Cu, Ge, Mo, Ni, Ce–Gd, Sm–Gd, Sn, and Y have been doped into $MgFe_2O_4$ crystal system [12, 13] by a variety of different techniques such as solid-state [5], combustion [14], melt quenching [15], sonochemical [16], hydrothermal [17], microemulsion, citrate-gel [18], and microwave [19]. Tetrazoles are nitrogen-rich chemical agents that have demonstrated various applications and gained great importance in organic

chemistry. For instance, a type of tetrazole compound derived from proline is a ligand that can be used in asymmetric and multicomponent reactions [20]. Hantzsch and Vagt [21] were the first researchers to disclose a common method for the synthesis of 5-aryl-1*H*-tetrazoles by cycloaddition of azide to match the nitrile (3 + 2) derivative. However, this type of reaction was cost-intensive and dangerous as it contains toxic, explosive, volatile, and water-sensitive compounds [22–24]. However, Demko and Sharpless [25] invented a safer aquatic approach using Zn salts as catalysts. Several compounds, including inorganic salts and metal complexes [26], $TMSN_3$, TBAF [27], $BF_3.OEt_2$ [23], $Pd(PPh_3)_4$ [28], $AlCl_3$ [29], $Yb(OTf)_3$ [30], $Zn(OTf)_3$ [31], $Pd(OAc)_2/ZnBr_2$ [32], and others, have been used as catalyst for the cycloaddition processes.

Homogeneous catalysts suffer from major challenges due to their separation and recycling difficulties. So, heterogeneous catalysts compensate for the above drawbacks and are considered a good alternative to them. Nanocrystalline Zn/Al HT, ZnO [33], Zn hydroxyapatite [34], Cu_2O [35, 36], $CdCl_2$ [37], $FeCl_3$-SiO_2 [38], natural natrolite zeolite [39], ZnS [40], and γ-Fe_2O_3 [41] are examples of heterogeneous catalysts. In the present study, following our efforts and interest in catalytic reactions [42–47] , $MgFe_2O_4$ and $MgFe_2Zn_xO_{4+\delta}$ nanoparticles are used as recyclable catalysts in the cycloaddition reaction between aryl nitrile and sodium azide to synthesize 5-aryl-1*H*-tetrazole compounds. In comparison with monometallic nanoparticle catalysts, the mixed metal oxide nanocatalysts have superior activity due to the cooperation nature of each of the metal oxides.

Experimental

Materials and procedures

Chemical compounds were bought from Merck and Aldrich suppliers and used at their standard purity. Their melting point was determined by the Philip Harris C4954718 apparatus. The infrared spectra were taken by a Thermo-Nicolet Nexus 670 FT-IR instrument over KBr discs. A Bruker Avance AQS 300 MHz spectrometer recorded ^{1}H NMR spectra. Chemical shifts were demonstrated by DMSO-d_6 in comparison with tetramethylsilane as the internal standard. The elemental Vario EL III elemental analyzer took the CHN analyses. The Brunauer-Emmett-Teller (BET) and the Barrett-Joyner-Halenda (BJH) methods were conducted to calculate surface area, pore-volume, and average particle size. The Beckman Coulter SA3100 surface area analyzer was used to save the data.

Synthesis of $MgFe_2O_4$ (S_1) and $MgFe_2Zn_xO_{4+\delta}$ (S_2)

The compounds were synthesized by the solid-state method described in the literature [48]. For the purpose, $MgCl_2.6H_2O$ (1 mmol, 203 mg) and $FeCl_3.6H_2O$ (2 mmol, 540 mg) were mixed in a mortar and ground until a homogenous powder was formed. The powder was placed into a crucible and treated thermally at 800 °C

for 12 h in order to complete the synthesis process in a pre-heated electrical furnace. The crucible was cooled down to room temperature in the furnace normally. For the $MgFe_2Zn_xO_{4+\delta}$ sample, $MgCl_2.6H_2O$ (1 mmol), $FeCl_3.6H_2O$ (2 mmol), and $Zn(NO_3)_2.6H_2O$ (0.034 mmol) were poured into a mortar and ground to obtain a homogeneous powder. The crucible was heated at 800 °C for 12 h in the preheated furnace. After the reaction was completed, the product mixture was allowed to cool down to room temperature in the furnace normally.

General process for the transformation of aromatic nitrile (ArCN) into compounds 4a-g

In order to perform a reflux process, all of the raw compounds included in Table 1 were mixed in a condenser and stirred for a certain time. Then, the prepared nanocatalyst (5 mol%) and DMSO (5 mL) were added to the mixture at 80 °C under an air atmosphere.

Reaction completion was monitored by a thin layer chromatography (TLC) test using an ethyl acetate/*n*-hexane (2:3 volume ratio) solvent mixture. The separation of the catalyst from the reaction mixture solution was done magnetically, and the catalyst recovery was done after the reaction's completion. Then, the solvent was removed from the product mixture by an evaporation process. The crude solid crystalline 5-aryl-1*H*-tetrazole was obtained by adding HCl (3 N, 10 mL) to the residue while vigorously stirring. Silica gel column chromatography was used to purify the product.

Results and discussion

Characterization

The as-prepared $MgFe_2O_4$ and $MgFe_2Zn_xO_{4+\delta}$ nanocomposites were characterized by the PXRD technique. Figure 1a, b shows the PXRD patterns of the obtained materials in the 2θ range of 10–80°. The results of structural analysis performed by the FullProf program employing profile matching with a constant scale factor are also included in the figures. The red lines are the observed intensities, while the black ones are the calculated data. The blue line is the difference: $Y_{obs} - Y_{calc}$. The Bragg reflection positions are indicated by blue, red, and green bars, which correspond to the main crystal phase ($MgFe_2O_4$) with space group Fd-3m and lattice parameters

Table 1 The precursors' chemical formulas to be applied in the reflux stage

Chemical formula	Quantity (mmol)
ArCN	1
NaN_3	1.5
NH_4OAc	1

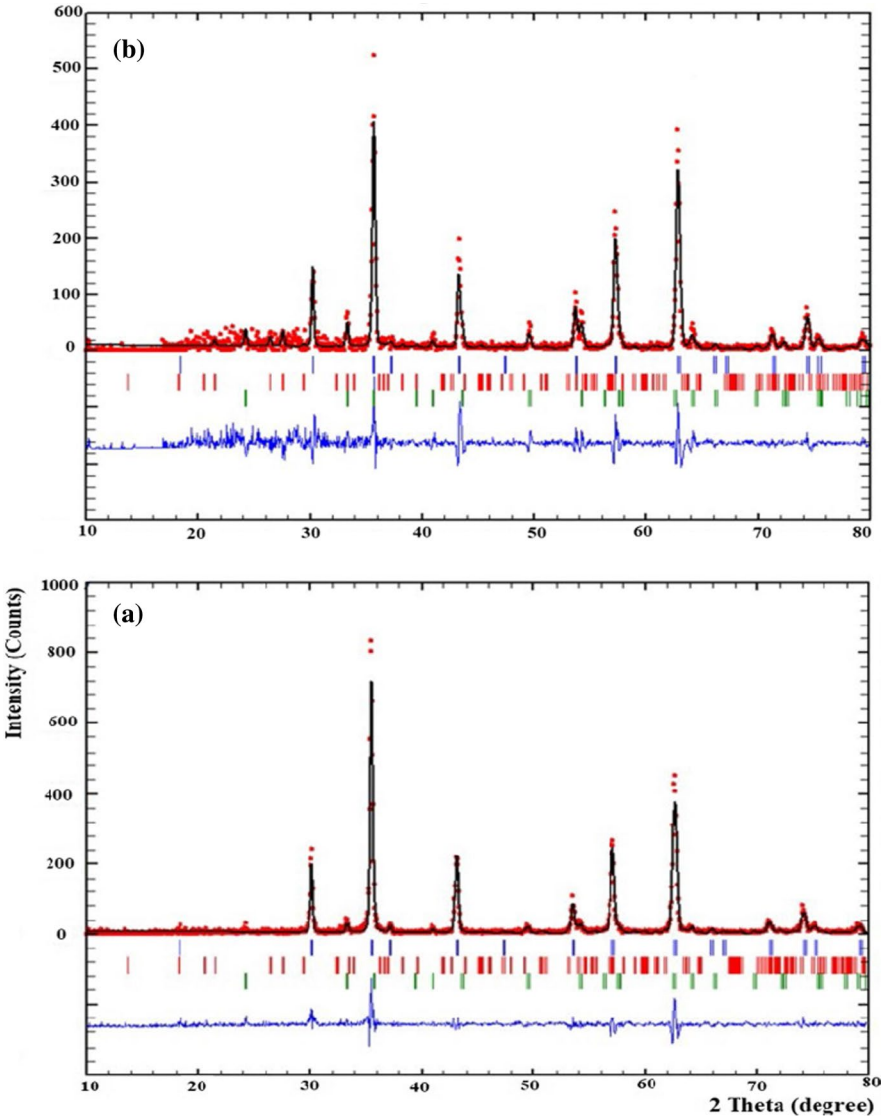

Fig. 1 PXRD patterns of S_1 **a** and S_2 **b**

of about $a=b=c=8.38$ Å [49–52], $MgFeO_3$ as a second crystal phase with space group C2/c and lattice parameters $a=9.72748$, $b=8.62991$ and $c=5.37184$ Å, and $\alpha=\gamma=90.0°$, and $\beta=90.03°$ [53], and Fe_2O_3 as a third and minimum crystal phase with space group *R*-3c and lattice parameters $a=b=5.02785$ and $c=13.73903$ Å and $\alpha=\beta=90.0°$ and $\gamma=120.0°$ [54], respectively. The crystallite sizes of S_1 and S_2 were calculated by the Scherrer equation using the peaks at 35.37 and 35.23°. The calculated grain sizes were 67 and 59 nm, respectively, for S_1 and S_2.

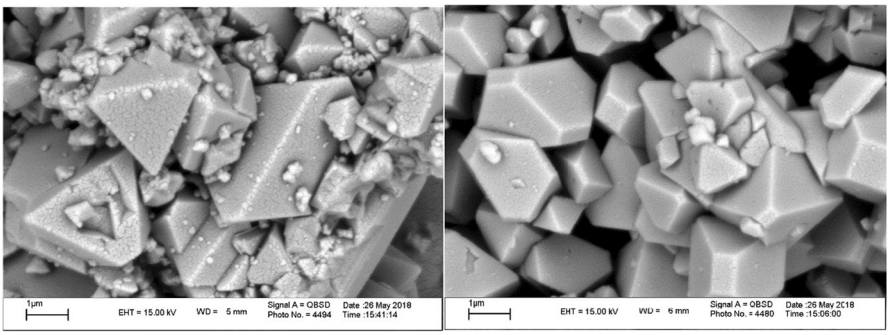

Fig. 2 FESEM images of left S_1 and right S_2

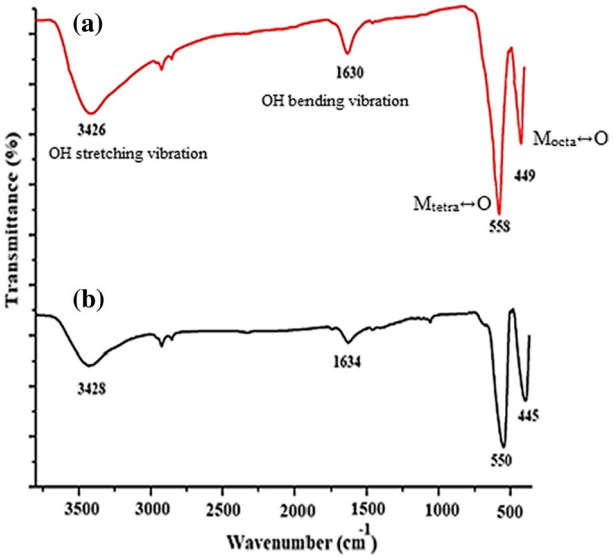

Fig. 3 FT-IR spectra of S_1 **a** and S_2 **b**

FESEM images of the fabricated samples are shown in Fig. 2. The images show that the morphology of the obtained samples is a prism with a homogeneous shape. However, it is found that S_2 has a more ordered shape than S_1. The particle sizes on the prisms are about 80–100 nm.

FT-IR spectra

The FTIR spectra of the prepared magnesium ferrite nanoparticles are illustrated in Fig. 3. The OH in the bending and stretching modes of water is revealed by the expanded bands at 1630 and 3426 cm^{-1}, respectively. The band at 558 cm^{-1} displays intrinsic metal atom stretching vibrations at the tetrahedral site, $M_{tetra} \leftrightarrow O$ (ν_1),

Table 2 BET data for $MgFe_2O_4$ and $MgFe_2Zn_xO_{4+\delta}$ show the textural attributes of the obtained materials

Sample	BET surface area ($m^2\ g^{-1}$)	Mean pore diameter (nm)	Pore volume ($cm^3\ g^{-1}$)
S_1	5.90	45	0.07
S_2	4.23	58	0.06

Table 3 BJH data for $MgFe_2O_4$ and $MgFe_2Zn_xO_{4+\delta}$ show the textural virtues of the obtained materials

Property	S_1	S_2
BJH surface area of pores ($m^2\ g^{-1}$)	6.37	4.01
BJH volume of pores ($cm^3\ g^{-1}$)	0.07	0.06
BJH average pore width (4 V/A) (nm)	33	45

whereas the band at 449 cm^{-1} (ν_2) band discloses metal-atom streching type vibration which is an octahedral bond, $M_{octa} \leftrightarrow O$. The longer and shorter bond lengths, related to oxygen–metal bands for octahedral Fe–O and tetrahedral Mg–O sites, can be associated with the discrepancy between two vibrations (ν_1 and ν_2) [55].

BET and BJH texture analysis

The produced powders surface area, average pore volume, and average pore size were investigated. The samples were degassed for 120 min at 150 °C in N_2 environment before measurement. Then, using N_2 adsorption–desorption isotherms at 77 K, the specific surface area (S_{BET}) of the collected samples was calculated. Table 2 presents the findings of the measurements. The surface area and the pore volumes of the targets are 5.90 to 4.23 $m^2\ g^{-1}$ and 0.07 to 0.06 $cm^3\ g^{-1}$, respectively (Table 3). Besides, the pore diameter sizes of the obtained materials are 45 and 58 nm for S_1 to S_2, respectively. BTH data are demonstrative of pore diameter value and in Table 3.

Magnetic property

Figure 4, shows the vibrating-sample magnetometer (VSM) data for the samples prepared by the solid-state method at room temperature. According to the figure, the values of saturation magnetization (M_s) change in the range of 24.4 (S_1) to 28.1 (S_2) emu/g. The data are reported associated with standard deviation (SD) values. The saturation values for the samples were higher than the values of 21.9 emu/g for sol–gel/combustion-synthesized $MgFe_2O_4$ [56] and 12.9 emu/g for co-precipitation-synthesized $MgFe_2O_4$ [5]. The outcomes revealed that the magnetic properties of the magnesium ferrite compounds have a direct correlation with the preparation technique. The magnetization strength of materials is defined by remnant magnetization Mr. This equals the magnetization that is retained when the external magnetic field reaches zero level ($H = 0$). The magnitudes of squareness are the ratio of the remnant per saturation magnetization ($M_{rs} = M_r/M_s$).

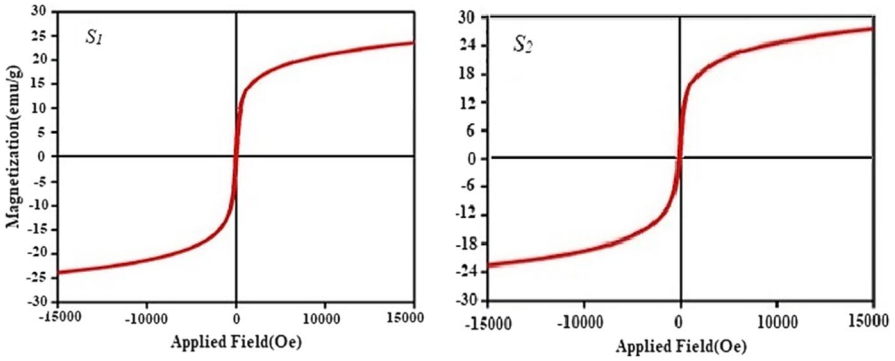

Fig. 4 M – H curves of as-synthesized nanomaterials at room temperature

Magnetic parameters are defined in Table 4 in which remanent magnetization, saturation magnetization, and coercive field strength corresponding to M_r, M_s, and H_c, respectively. The squareness ratio will be less than 0.5 when a particle has an isotropic distribution and uniform magnetization without intergrain interactions. The formation of a multi-domain structure over the exchange coupling between adjacent grains explains this value. Because the value of M_{rs} is 0.11, it can be seen that the samples have no preferred magnetization direction and show a typical (*S*-shaped) narrow hysteresis loop. A low coercivity rating is shown by the narrow loop. As a result, the demagnetization of the prepared samples is simple.

During the preparation of 5-aryl-1*H*-tetrazoles using benzonitrile derivatives, the performance of the synthesized nanoparticles was analyzed for their catalytic activity (Scheme 1). The optimization was carried out to improve reaction efficacy. ArCN reaction using NaN_3 and different solvents was carried out by helping the prepared catalyst (5 mol%, Table 5). Organic compounds such as Tetrahydrofuran (THF), Dimethyl sulfoxide (DMSO), Dimethylformamide (DMF), dioxane, toluene, and water were also used as solvent in the catalytic reactions. According to Table 5, DMSO is the most suitable solvent to obtain the maximum yield (Table 5, entry 9).

Table 5, entries 6–10, clarifies the temperature role in the reaction yield. To do the reactions, the catalytic process was started at room temperature and then, the reactions were performed at 40, 60, 80, and 100 °C, distinctly, to find the optimum temperature condition. The data revealed that the reaction yield maximized at 80 °C and remained nearly constant at higher temperatures. Finding the best catalyst quantity for the reaction is the subsequent stage. The procedure was

Table 4 The magnetic hysteresis parameters of the prepared samples

Sample	M_r (emu/g) (SD)	M_s (emu/g) (SD)	$M_{rs}=M_r/M_s$ (SD)	H_c (Oe) (SD)
S_1	2.9 (±0.1)	24.4 (±0.1)	0.119 (±0.02)	50.9 (±0.1)
S_2	3.2 (±0.1)	28.1 (±0.1)	0.114 (±0.02)	53.4 (±0.1)

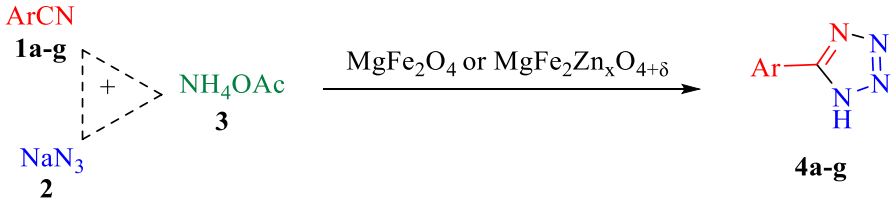

a; Ar = C_6H_5 **b**; Ar = 4-BrC_6H_4 **c**; 4-ClC_6H_4 **d**; 4-MeC_6H_4
e; Ar = 4-$MeOC_6H_4$ **f**; 3-$O_2NC_6H_4$ **g**; 4-HOC_6H_4

Scheme 1 Preparation of 5-aryl-1*H*-tetrazoles catalyzed by S_1 or S_2 nanoparticles

Table 5 Conditions improvement for the preparation of 5-phenyl-1*H*-tetrazol*

Entry	Catalyst (mol%)	Solvent	Temperature (°C)	Time (h)	Yield (%)
1	5	THF	Reflux	3	12
2	5	DMF	100	3	23
3	5	Dioxane	Reflux	3	10
4	5	Toluene	Reflux	3	18
5	5	H_2O	Reflux	9	26
6	5	DMSO	RT	3	57
7	5	DMSO	40	3	71
8	5	DMSO	60	3	79
9	**5**	**DMSO**	**80**	**3**	**97**
10	5	DMSO	100	3	97
11	–	DMSO	80	6	–
12	2	DMSO	80	3	49
13	10	DMSO	80	3	97

*The reaction of benzonitrile (**1a**, 1 mmol), NaN_3 (**2**, 1.5 mmol), NH_4OAc (**3**, 1 mmol), and $MgFe_2O_4$ (5 mol%), in solvent (5 mL)

carried out under the following optimum temperature at the absence and presence of nanocatalyst (2, 5 and 10 mol%): The best results are shown at 5 mol% (Table 5, entries 9–13).

The concept of the catalytic mode on the respective tetrazoles ring preparation from benzonitrile derivatives was tested using optimum reaction conditions. The activity of nitrile compounds toward azide ions in cycloaddition reaction is crucial. Empirically, we found that aryl nitriles with electron-withdrawing groups raise the polarity of the cyanide group inductively leads to higher yields within a shorter time of reaction than other nitrile compounds (Table 6, entry 6). According to the data included in Table 6, when a reactant that possesses an electron-donating agent (methyl/methoxy/hydroxy) is utilized in the reaction mixture, the tetrazole derivative compound is produced in a high yield (entries 4, 5 and 7) at a longer reaction

Table 6 A comparison study between S_1 and S_2 for the synthesis of 5-aryl-1*H*-tetrazoles derivatives*

Entry	Ar	Product	Time (h)	Yield (%)	M.p. (°C)	
				S_1 S_2	Found	Lit
1	C_6H_5	**4a**	3	97 98	213–216	215–216 [57]
2	4-BrC_6H_4	**4b**	3	92 93	266–269	267–269 [35]
3	4-ClC_6H_4	**4c**	3	93 94	260–262	261–263 [57]
4	4-MeC_6H_4	**4d**	4	89 90	246–248	248–250 [58]
5	4-$MeOC_6H_4$	**4e**	4	87 89	232–233	231–232 [25]
6	3-$O_2NC_6H_4$	**4f**	2	97 98	218–221	219 [58]
7	4-HOC_6H_4	**4g**	4	87 88	232–235	234–235 [57]

*Reaction conditions: Benzonitrile derivative (**1a–g**, 1 mmol), NaN_3 (**2**, 1.5 mmol), NH_4OAc (**3**, 1 mmol), and $MgFe_2O_4$ (5 mol%), in DMSO (5 mL) at 80 °C

time duration. Benzonitriles with halogen substituents (4-Cl and 4-Br) interacted smoothly and produced the desired results (Table 6, entries 2 and 3). The data included in Table reveal that the efficiency of S_2 is more than S_1 at the optimum reaction conditions.

As shown in Scheme 2, an appropriate route for the synthesis of 5-aryl-1*H*-tetrazoles using the prepared nanocatalysts is proposed. Intermediate I is formed by the coordination of nitrogen atom in nitrile group of Ar-CN 1a–g with Mg(II), which speeds up the cyclization process. This claim was supported by the observation when the reaction was performed without the presence of $MgFe_2O_4$. Even after a long period of time, the cycloaddition reaction without a catalyst did not complete (Table 5, entry 11). The intermediate II was generated via a concerted [3 + 2] cycloaddition reaction of the nitrile's group with azide ion. The desired tetrazoles

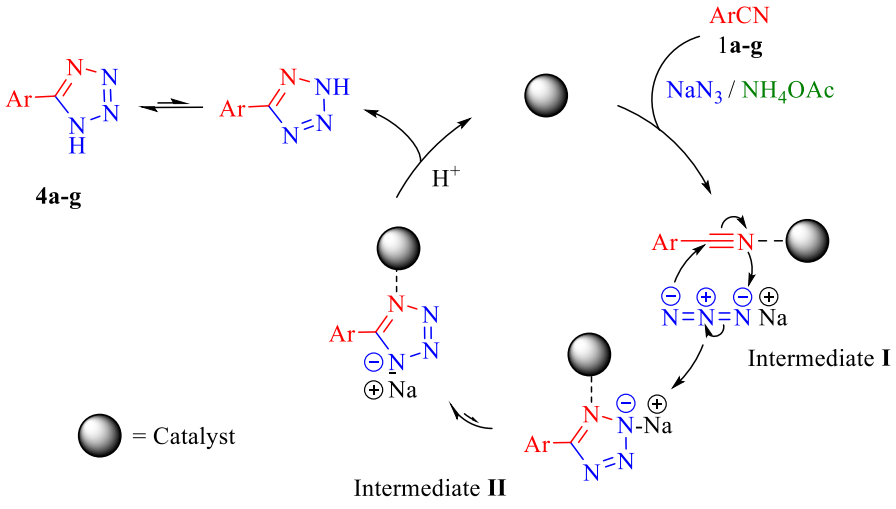

Scheme 2 A proposed pathway for the formation of compounds 4**a–g**

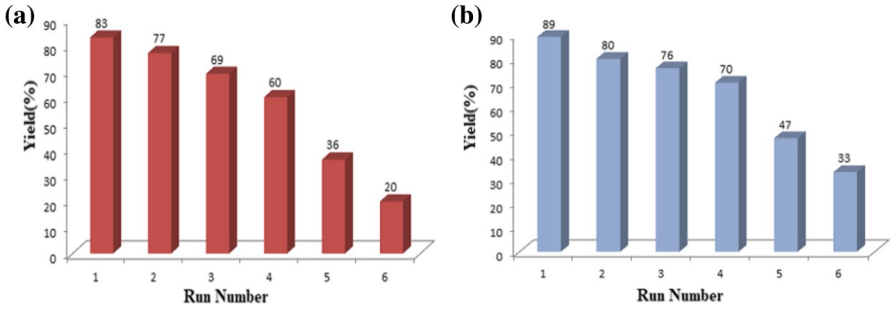

Fig. 5 Reusability comparison between S_1 **a** and S_2 **b**

4a–g as final product and $MgFe_2O_4$ catalyst were obtained by protonolysis of intermediate II with NH_4OAc H^+ or extraction using hydrochloric acid. Ammonium acetate can form ammonium azide in situ by reacting it with sodium azide, which increases the accessibility of the N_3^- for cycloaddition with C≡N, and it can also be utilized as a proton source into the corresponding tetrazoles [59–61].

During the tetrazole ring formation under the optimum conditions, the catalyst ($MgFe_2O_4$) recovery and reusability were studied. When the benzonitrile-sodium azide reaction was completed, the catalyst was isolated from the reaction mixture by applying an external magnet, washed with acetone and then water, and kept in an oven at 120 °C for 4 h. The reusability of the catalyst was tested by repeating the reaction until the yield decreased considerably. It is worth noting that the recovered catalyst maintains its peak up to a 4 s run (Fig. 5).

In Fig. 6, the PXRD pattern of S_2 after 4 runs of catalytic reaction is presented. It is found that the catalyst suffers from crystal phase decreases. Besides, it is clear that the impurity phases, including $MgFeO_3$ and Fe_2O_3, increase.

The efficiency of the catalyst was assessed by comparing it to that of other heterogeneous catalytic systems which demonstrates its priority over other systems in the literature (Table 7).

Conclusion

In this study, magnesium ferrite and Zn-doped samples were synthesized by the solid-state method and used as effective heterogeneous catalysts for [3 + 2] cycloaddition reactions of benzonitriles with azide as the starting material to give 5-aryl-1*H*-tetrazoles with high yields. FESEM images showed that the morphology of the prepared samples was prism. The VSM data revealed that the samples had ferromagnetic properties with a considerable saturation magnetization of 28 emu/g. The data showed that the optimum reaction temperature was 80 °C when DMSO was used as the reaction mixture solvent. A high reaction yield (97%) was obtained when 5 mol% of the prepared nanocatalyst was used. Separation and recovery of the catalyst from the reaction solution were done easily by an external magnet. The reaction was feasible for four successive runs without a noticeable fall in catalytic activity.

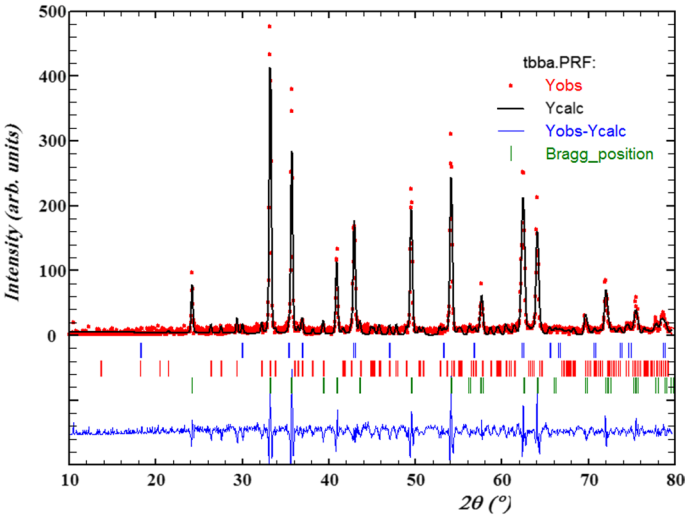

Fig. 6 PXRD pattern of S_2 after 4 runs of the catalytic reaction

Table 7 Different heterogeneous catalysts comparison in the formation of compound **4a**

Entry	Catalyst	Temperature (°C)	Time (h)	Yield (%)	Lit
1	Nano-ZnO	120	14	72	[62]
2	$CuFe_2O_4$	120	12	82	[63]
3	$NiFe_2O_4$	100	3	94	[64]
4	Cu_2O	230	7	74	[65]
5	nano-$TiCl_4.SiO_2$	Reflux	1.5	95	[66]
6	$FeCl_3.SiO_2$	120	12	79	[67]
7	$Cu(NO_3)_2.3H_2O$	120	16	92	[38]
8	$CuWO_4.2H_2O$	120	24	72	[68]
9	GO/ZnO	120	30	78	[41]
10	$MgFe_2O_4$	80	3	97	Current study
11	$MgFe_2Zn_xO_{4+\delta}$	80	3	98	Current study

Supplementary Information The online version contains supplementary material available at https://doi.org/10.1007/s11164-022-04741-6.

Acknowledgements The authors are grateful to Urmia University for supporting this research.

References

1. Z. Zhuang, D. Liu, Nano-Micro Lett. **12**, 1 (2020)
2. S. Kumar, S. Jain, M. Nehra, N. Dilbaghi, G. Marrazza, K.H. Kim, Coord. Chem. Rev. **420**, 213407 (2020)
3. M.A. Ashraf, Z. Liu, C. Li, D. Zhang, Appl. Organomet. Chem. **35**, e6133 (2021)

4. K. Kirchberg, A. Becker, A. Bloesser, T. Weller, J. Timm, C. Suchomski, R. Marschall, J. Phys. Chem. C. **121**, 27126 (2017)
5. Z. Wang, P. Lazor, S.K. Saxena, H.S.C. O'Neill, Mater Res. Bull. **37**, 1589 (2002)
6. Z.J. Zhang, Z.L. Wang, B.C. Chakoumakos, J.S. Yin, J. Am. Chem. Soc. **120**, 1800 (1998)
7. S.A. Oliver, R.J. Willey, H.H. Hamdeh, G. Oliveri, G. Busca, Scr. Mater. **33**, 1695 (1995)
8. D.H.K. Reddy, Y.S. Yun, Coord. Chem. Rev. **315**, 90 (2016)
9. N. Kaur, M.M. Kaur, Process Appl. Ceram. **8**, 137 (2014)
10. S.M. Yakout, M.R. Hassan, M.I. Aly, Water Sci. Technol. **77**, 2714 (2018)
11. A. Sankaramahalingam, J.B. Lawrence, Synth. React. Inorg. Met. **42**, 121 (2012)
12. N.M. Deraz, O.H. Abd-Elkader, Int. J. Electrochem. Sci. **8**, 8632 (2013)
13. S.M. Hoque, M.A. Hakim, A. Mamun, S. Akhter, M.T. Hasan, D.P. Paul, K. Chattopadhayay, Mater Sci. Appl. **2**, 1564 (2011)
14. Y.S.Z. Rúbia, G.K. Claudir Jr., K.A. Annelise, P.B. Carlos, FME Trans. **46**, 157 (2018)
15. S.E. Shabrawy, C. Bocker, C. Rüssel, Solid State Sci. **60**, 85 (2016)
16. M.I.M. Omer, A.A. Elbadawi, O.A. Yassin, J. Appl. Ind. Sci. **1**, 20 (2013)
17. S. Ilhan, S.G. Izotova, A.A. Komlev, Ceram Int. **41**, 577 (2014)
18. M.E. Rabanal, A. Varez, B. Levenfeld, J.M. Torralba, Bol. Soc. Esp. Ceram Vidrio. **39**, 277 (2000)
19. T. Iwamoto, Y. Komorida, M. Mito, A. Takahara, J. Coll. Interface. Sci. **345**, 143 (2010)
20. R.N. Butler, A.R. Katritzky, C.W. Rees, E.F.V. Scriven (eds.), *Comprehensive Heterocyclic Chemistry* (Pergamon, Oxford, UK, 1996)
21. A. Hantzsch, A. Vagt, Justus Liebigs Ann. Chem. **314**, 339 (1901)
22. D.P. Curran, S. Hadida, S.-Y. Kim, Tetrahedron. **55**, 8997 (1999)
23. A. Kumar, R. Narayanan, H. Shechter, J. Org. Chem. **61**, 4462 (1996)
24. K. Koguro, T. Oga, S. Mitsui, R. Orita, Synthesis. **6**, 910 (1998)
25. Z.P. Demko, K.B. Sharpless, J. Org. Chem. **66**, 7945 (2001)
26. J. Bonnamour, C. Bolm, Chem.Eur. J. **15**, 4543 (2009)
27. D. Amantini, R. Beleggia, F. Fringuelli, F. Pizzo, L. Vaccoro, J. Org. Chem. **69**, 2896 (2004)
28. Y.S. Gyoung, J.-G. Shim, Y. Yamamoto, Tetrahedron Lett. **41**, 4193 (2000)
29. D.P. Matthews, J.E. Green, A.J. Shuker, J. Comb. Chem. **2**, 19 (2000)
30. W.K. Su, Z. Hong, W.G. Shan, X.X. Zhang, Eur. J. Org. Chem. **2006**, 2723 (2006)
31. S. Hajra, D. Sinha, M. Bhowmick, J. Org. Chem. **72**, 1852 (2007)
32. Z. Yizhong, R. Yiming, C. Chun, Helv. Chim. Acta. **92**, 171 (2009)
33. M.L. Kantam, K.B.S. Kumar, K.P. Raja, J. Mol. Catal. A. **247**, 186 (2006)
34. M.L. Kantam, V. Balasubrahmanyam, K.B.S. Kumar, Synth. Commun. **36**, 1809 (2006)
35. T. Jin, F. Kitahara, S. Kamijo, Y. Yamamoto, Tetrahedron Lett. **49**, 2824 (2008)
36. T. Jin, F. Kitahara, S. Kamijo, Y. Yamamoto, Chem. Asian J. **3**, 1575 (2008)
37. G. Venkateshwarlu, A. Premalatha, K.C. Rajanna, P.K. Saiprakash, Synth. Commun. **39**, 4479 (2009)
38. M. Nasrollahzadeh, Y. Bayat, D. Habibi, S. Moshaee, Tetrahedron Lett. **50**, 4435 (2009)
39. M. Nasrollahzadeh, D. Habibi, Z. Shahkarami, Y. Bayat, Tetrahedron. **65**, 10715 (2009)
40. L. Lang, B. Li, W. Liu, L. Jiang, Z. Xu, G. Yin, Chem. Commun. **46**, 448 (2010)
41. G. Qi, Y. Dai, Chin. Chem. Lett. **21**, 1029 (2010)
42. M. Aslanpanjeh, A.P. Marjani, J. Khalafy, N. Etivand, Res. Chem. Intermed. **46**, 165 (2020)
43. A. Nouri, A.P. Marjani, J. Khalafy, N. Etivand, Res. Chem. Intermed. **46**, 3025 (2020)
44. L. Kafi-Ahmadi, A.P. Marjani, E. Nozad, Appl. Organomet. Chem. **35**, e6271 (2021)
45. F. Majidi Arlan, A.P. Marjani, R. Javahershenas, J. Khalafy, New J. Chem. **45**, 12328 (2021)
46. F. Azimi, A.P. Marjani, S. Keshipour, Sci. Rep. **11**, 23769 (2021)
47. B.P. Habashi, A.P. Marjani, Res. Chem. Intermed. **48**, 2325 (2022)
48. F. Yousefzadeh, L. Kafi-Ahmadi, Sh. Khademinia, Catal. Lett. **149**, 1660 (2019)
49. H. Das, T. Arai, N. Debnath, N. Sakamoto, K. Shinozaki, H. Suzuki, N. Wakiya, Adv. Powder Technol. **27**, 541 (2016)
50. J. Nonkumwong, P. Pakawanit, A. Wipatanawin, P. Jantaratana, S. Ananta, L. Srisombat, Mater. Sci. Eng. C. **61**, 123 (2016)
51. C. Fragassa, L. Berardi, G. Balsamini, FME Trans. **44**, 333 (2016)
52. A. Ivanets, M. Roshchina, V. Srivastava, V. Prozorovich, T. Dontsova, S. Nahirniak, V. Pankov, A. Hosseini-Bandegharaei, H.N. Tran, M. Sillanpää, Colloids Surf. A Physicochem. Eng. Asp. **571**, 17 (2019)

53. N.T. Hung, L.H. Bac, N.N. Trung, N.T. Hoang, P.V. Vinh, D.D. Dung, J. Magn. Magn. Mater. **451**, 183 (2018)
54. S. Zhang, X.J. Chen, C.R. Gu, Y. Zhang, J.D. Xu, Z.P. Bian, D. Yang, N. Gu, Nanoscale Res. Lett. **4**, 70 (2009)
55. H. Kavas, N. Kasapoğlu, A. Baykal, Y. Köseoğlu, Chem. Pap. **63**, 450 (2009)
56. A. Pradeep, P. Priyadharsini, G. Chandrasekaran, J. Magn. Magn. Mater. **320**, 2774 (2008)
57. V. Rama, K. Kanagaraj, K. Pitchumani, J. Org. Chem. **76**, 9090 (2011)
58. L.V. Myznikov, A. Hrabalek, G.I. Koldobskii, Chem. Heterocycl. Chem. **43**, 1 (2007)
59. M. Nasrollahzadeh, B. Jaleh, A. Jabbari, RSC Adv. **4**, 36713 (2014)
60. D.R. Patil, M.B. Deshmukh, D.S. Dalal, J. Iran. Chem. Soc. **9**, 799 (2012)
61. H. Sharghi, S. Ebrahimpour Moghaddam, M.M. Doroodmand, J. Organomet. Chem. **738**, 41 (2013)
62. B. Sreedhar, A.S. Kumar, D. Yada, Tetrahedron Lett. **52**, 3365 (2011)
63. M. Lakshmi Kantam, K.B. Shiva Kumar, C. Sridhar, Adv. Synth. Catal. **347**, 1212 (2005)
64. B. Sreedhar, A.S. Kumar, D. Yada, Tetrahedron Lett. **52**, 3565 (2011)
65. F. Abrishami, M. Ebrahimikia, F. Rafiee, Appl. Organometal. Chem. **29**, 730 (2015)
66. S.M. Joshi, R.B. Mane, K.R. Pulagam, V. Gomez-Vallejo, J. Llop, C. Rode, New J. Chem. **41**, 8084 (2017)
67. L. Zamani, B.B.F. Mirjalili, K. Zomorodian, S. Zomorodian, S. Afr, J. Chem **68**, 133 (2015)
68. C. Tao, B. Wang, L. Sun, J. Yi, D. Shi, J. Wang, W. Liu, J. Chem. Res. **41**, 25 (2016)